

UC Davis

UC Davis Previously Published Works

Title

In situ polymerized PEDOT dispersions with sulfated cellulose nanofibrils for 1D and 2D conductors

Permalink

<https://escholarship.org/uc/item/08r9b7tx>

Journal

Materials Advances, 4(20)

ISSN

2633-5409

Authors

Pingrey, Benjamin

Hsieh, You-Lo

Publication Date

2023-10-16

DOI

10.1039/d3ma00486d

Copyright Information

This work is made available under the terms of a Creative Commons Attribution-NonCommercial License, available at <https://creativecommons.org/licenses/by-nc/4.0/>



Peer reviewed

PAPER



Cite this: *Mater. Adv.*, 2023,
4, 4912

In situ polymerized PEDOT dispersions with sulfated cellulose nanofibrils for 1D and 2D conductors†

Benjamin Pingrey ^a and You-Lo Hsieh ^{*ab}

Sulfated cellulose nanofibrils (SCNFs, 1.7 ± 0.7 nm high, 3.6 ± 0.9 nm wide, 880 ± 320 nm long) with 1.81 mmol g^{-1} surface charge or ca. 84% C6 sulfation have shown to be effective co-polyelectrolytes with poly(styrene sulfonate) (PSS) in the synthesis of poly(3,4-ethylenedioxythiophene) (PEDOT). Stable aqueous dispersions of PEDOT:PSS/SCNF were synthesized with up to 50 wt% PEDOT fractions in the presence of any combination of SCNF and/or PSS as co-polyelectrolytes. The closely matched spacing between the SCNF anionic groups and PEDOT cationic groups facilitated the alignment of PEDOT along the surface of nanofibrils to enhance conductivity of 2D cast films and 1D wet spun fibers to 0.14 S cm^{-1} and 40 S cm^{-1} , respectively. Ethylene Glycol (EG) further acted on the PSS in the PEDOT:PSS/SCNF complexes to improve the conductivity of films to a maximum of 37.5 S cm^{-1} and that of fibers to 6150 S cm^{-1} . Most impressively, wet spinning PEDOT:PSS/SCNF with 30% SCNF in the polyanions directly into 72% sulfuric acid yielded fibers with an even higher conductivity of $15\,500 \pm 3500$ S cm^{-1} .

Received 31st July 2023,
Accepted 20th September 2023

DOI: 10.1039/d3ma00486d

rsc.li/materials-advances

Introduction

Poly(3,4-ethylene dioxythiophene) (PEDOT), a 3,4-disubstituted polythiophene conducting polymer, has attracted great interest for research and gained widespread commercial success since its discovery in 1988.¹ PEDOT differentiates itself from other intrinsically conducting polymers (ICPs) in many aspects. First, PEDOT is more conductive than polyphenylenes by approximately an order of magnitude.² It is safer to manufacture than polypyrrole due to the lower toxicity and volatility of the EDOT monomer compared to pyrrole.³ PEDOT is also relatively stable under atmospheric conditions, greatly eclipsing the extremely unstable yet highly conductive polyacetylene. Furthermore, PEDOT exhibits stable conductivity at temperatures of up to 280 °C, significantly higher than polypyrrole and polyaniline as well as above the temperatures needed when using lead free solder.³ This allows PEDOT to be incorporated into components such as electrolytic capacitors without risking thermal degradation due to soldering.⁴

Most uniquely, PEDOT can be made aqueous dispersible due to its ability to form stable polyelectrolyte complexes, facilitating direct processing. On its own, PEDOT is insoluble

in any known solvent, and therefore processing pure PEDOT into films requires either chemically or electrochemically polymerizing it onto a surface. This issue was circumvented with the discovery that PEDOT can be polymerized in the presence of a host polyelectrolyte, typically poly(styrene sulfonate) (PSS), to form stable aqueous dispersions. In these PEDOT:PSS polyelectrolyte complexes, positive charges formed during oxidation of the PEDOT chain—analogueous to p-type doping in traditional semiconductors—are electrostatically bound to the PSS anionic sulfonate groups.³ These dispersions are attractive from an engineering point of view because they allow PEDOT be processed using a myriad of well-established solution-based techniques, including spin coating,⁵ doctor blading,⁶ dip coating,⁷ drop casting,⁸ ink-jetting,⁹ and wet spinning.¹⁰ However, the most widely studied aqueous PEDOT dispersions have a 2.5 : 1 PSS : PEDOT mass ratio, containing 71 wt% of insulating PSS that has a profound effect on the resulting conductivity.

Improving the conductivity of PEDOT:PSS has therefore been a critical topic of research, with numerous strategies reported. The most prolific method of enhancing the conductivity of PEDOT:PSS is the use of so-called secondary dopants¹¹ or conductivity enhancement agents.³ These chemicals are commonly high boiling point solvents, such as dimethyl sulfoxide (DMSO) or ethylene glycol (EG), which are added to PEDOT:PSS dispersions prior to processing and are often (but not always^{12,13}) removed from the final product during curing.¹⁴ It should be noted that the term secondary doping, while widely used for an agent used for improving conductivity, does not imply a change in

^a Chemical Engineering, Davis, California 95616-8722, USA

^b Biological and Agricultural Engineering University of California at Davis, Davis, California 95616-8722, USA. E-mail: ylhsieh@ucdavis.edu

† Electronic supplementary information (ESI) available. See DOI: <https://doi.org/10.1039/d3ma00486d>

the electronic structure of the PEDOT itself, as is the case in p- or n-type doping of traditional semiconductors. In conducting polymers, doping generally refers to redox reactions that create positive or negative charges along the polymeric chain.³ The species created in these redox reactions—predominantly bipolarons in the case of PEDOT—lead to additional valid energy levels in the band gap of the polymer that dramatically increase conductivity.¹⁵ In PEDOT:PSS, secondary dopants bring about no oxidative nor electronic change and, in many cases, are not even present in the final material. Despite this fact, the application of so-called secondary dopants is known to drastically increase conductivity, by as much as 2–3 orders of magnitude.¹⁴ The exact mechanism of this enhancement, however, remains a topic of great debate. One proposed explanation is that the enhancement results from small remaining dopant in the film to screen electrostatic interactions between PEDOT and PSS with their polar moieties.¹⁶ Another postulates that the additives act as plasticizers, facilitating the reorganization of PEDOT chains and their phase-separation from PSS in a manner that leads to larger PEDOT-rich domains with reduced resistance and, in turn, higher conductivity.¹⁷ Other explanations include the removal of the non-conductive PSS during secondary doping¹⁸ or the conformational change in PEDOT from a benzoid to a planar quinoid structure whose conjugated backbone is favored for higher conductivity.¹⁹ On account of both their effectiveness and ubiquity, better understanding the mechanisms of secondary dopants in enhancing the conductivity of hybrid PEDOT structures warrants more in-depth investigation.

The conductivity of the inherently heterogeneous PEDOT:PSS complexes depends as much on ordering and supramolecular structure of both PEDOT and PSS as it does on factors like degree of polymerization or doping level. To that effect, the conductivity of PEDOT:PSS complexes has been improved by manipulating their morphology through the incorporation of cellulose nanofibrils (CNF)—1D nanomaterials formed by breaking down cellulose through a combination of chemical and mechanical treatments.²⁰ The inclusion of carboxymethylated CNF with PEDOT:PSS has been shown to enhance pi-stacking of PEDOT along the nanofibrils, increasing conductivity of films treated with glycerol to 400 S cm^{-1} ; a $2.6\times$ increase over using dissolved carboxymethyl cellulose.²¹ Similarly, a 2-fold increase in conductivity from 18.8 S cm^{-1} to 40.8 S cm^{-1} has been shown for films cast with PEDOT:PSS (Clevios PH1000) mixed with carboxylated CNF from TEMPO-mediated oxidation, despite the fact that the overall PEDOT fraction was reduced with the insulating CNF.²² Mixing commercial PEDOT:PSS with sulfated cellulose nanofibrils from sulfuric acid treatment has also increased the conductivity of films produced from 1000 to 2500 S cm^{-1} .²³ PEDOT dispersions have also been formed without any PSS by polymerizing PEDOT in the presence of sulfated cellulose nanofibrils (SCNF) produced through sulfamic acid treatment and homogenization.²⁴ Notably, these PEDOT:SCNF dispersions remained stable even at relatively high PEDOT concentrations up to 50 wt%, or 1:1 mass ratio, higher than using PSS as the lone dispersant. However, the conductivities of films made from the PEDOT:SCNF dispersions were relatively low, capping

out at 1.89 S cm^{-1} . While incorporating CNFs as templating materials with^{21–23} or for the synthesis²⁴ of PEDOT has shown some promise in improving its conductivity, many questions persist about the specific functionalized CNFs and the behavior and properties of systems in which PEDOT is complexed with. For instance, in templating works utilizing CNFs in conjunction with commercial PEDOT:PSS, the carboxymethyl,²¹ carboxylated,²² and sulfated²³ CNFs were synthesized with different starting materials, reagents, and procedures, leading to varied nanofibril dimensions, crystallinity, and degrees and chemical functionalization for understanding of templating approach or direct comparisons. Additionally, the extent to which secondary dopants affect PEDOT dispersions containing CNF in place of PSS has not been attempted.

This study aims to exploit the *in situ* polymerization of EDOT approach systematically by using a well-defined SCNF as the lone host polyelectrolyte as well as in conjunction with PSS. Sulfated cellulose nanofibrils (SCNFs) bearing 1.8 mmol g^{-1} of sulfate groups have been robustly produced through the reaction with chlorosulfonic acid in anhydrous *N,N*-dimethylformamide (DMF) followed by high-speed blending.²⁵ EDOT was polymerized into PEDOT in the presence of anionic SCNF and/or PSS polyelectrolytes in varying ratios to investigate the stability and properties of the aqueous PEDOT:PSS/SCNF dispersions produced and the morphology and conductivity of films as functions of aqueous PEDOT:PSS/SCNF dispersion compositions. The effect of secondary doping with EG and DMSO on PEDOT:SCNF and hybrid PEDOT:PSS/SCNF systems was examined to maximize the conductivity of films and to discern the potential doping mechanism. Shear-mediated orientation of SCNF-associated PEDOT was investigated by wet spinning aqueous PEDOT:PSS/SCNF into fibers to study its effect to further improve conductivity and the doping effect of EG applied in the vapor phase.

Results & discussion

SCNF properties

Sulfated cellulose nanofibrils (SCNFs) were robustly produced by sulfation of dissolving pulp using chlorosulfonic acid (1.25 moles per AGU, 45 min) in anhydrous DMF and aqueous disintegration *via* high-speed blending (30 000 rpm, 10 min) in 99% yield. These SCNFs were $1.7 \pm 0.7 \text{ nm}$ high (H) and $880 \pm 320 \text{ nm}$ long (L), measured by AFM, and $3.6 \pm 0.9 \text{ nm}$ wide (W), measured by TEM (Fig. 1). SCNFs exhibited anisotropic cross-sections with an average 2.1 W/H ratio and high 244 L/W or 518 L/H aspect ratios. The concentration of surface sulfate half-ester groups (R-OSO_3^-) was $1.81 \pm 0.09 \text{ mmol per gram of SCNF}$. The nanofibrils had a crystallinity index (CrI) of 0.58 (Fig. S1, ESI[†]), down from 0.78 of the starting dissolving pulp cellulose due to robust conversion of pulp cellulose to SCNF *via* sulfation with chlorosulfonic acid.

Based on the SCNF cross-sectional dimensions and a crystalline model established previously,²⁵ *ca.* 28% of all surface C2, C3, and C6 hydroxyl groups were sulfated. Assuming sulfation of cellulose chains in the non-crystalline region *via* chlorosulfonic

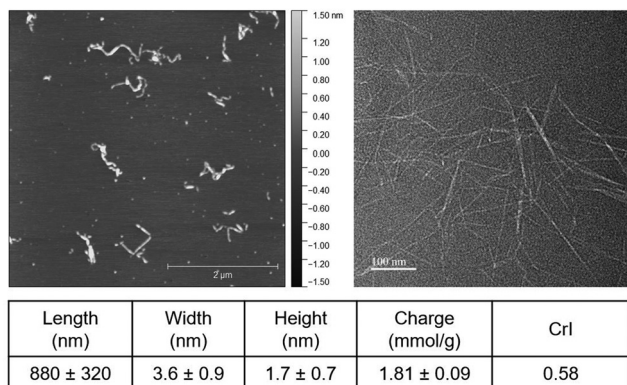


Fig. 1 AFM (left) and TEM (right) of SCNF with dimensions and properties in table below.

acid to occur preferentially at the C6 position as in dissolved cellulose,²⁶ 84% of surface C6 hydroxyls are estimated to be sulfated. Adjacent C6 hydroxyls on a nanofibril's surface are located every other anhydroglucose unit 10.38 Å apart (Fig. 2). Dividing this adjacent C6 OH spacing by the estimated percentage of C6 surface sulfation to factor in unfunctionalized sites, the estimated average charge spacing for the SCNF is 12.3 Å. Doped PEDOT is found to carry approximately one positive charge per three thiophene rings³ and has a repeating unit length of 3.963 Å,²⁷ leading to an average charge spacing of 11.89 Å; reasonably close to the 12.3 Å spacings of sulfated charge sites along SCNF. The close match between the 12.3 Å anionic C6 surface sulfate spacings on SCNF surface and the 11.89 Å PEDOT cation charge groups leads to ramifications for how PEDOT polymer chains form polyelectrolyte complexes along SCNF surfaces. Two molecular arrangements for polyelectrolyte complexes are typically discussed: the ladder type, where polycation and polyanion chains are paired more parallel to each other, and the “scrambled egg” type based on more random pairing between multiple polycation and polyanion chains.³ While most polyelectrolyte complexes exist somewhere between these two extremes, similar charge spacing between the polycation

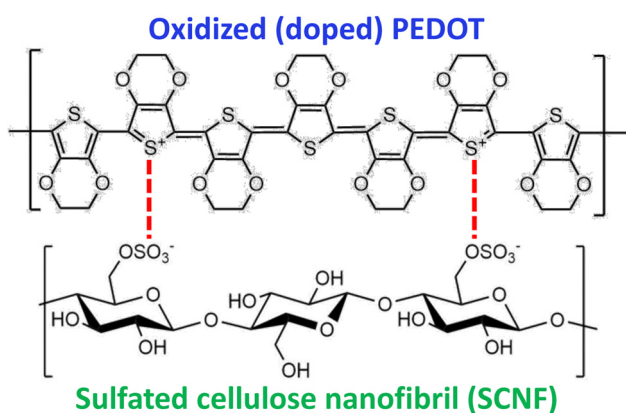


Fig. 2 Polyelectrolyte complex of doped PEDOT cations (top) with sulfated SCNF surface anions (bottom).

and polyanion and a large discrepancy between the molecular weights of the two polymers have shown to favor the more organized ladder-like structure.²⁸ The 1D anisotropic SCNF, being an average of 880 nm long, possess vastly larger dimensions than PEDOT, which typically has very low molecular weights of several kDa, or around a dozen monomeric units.³ Both factors—*i.e.*, closely matched spacings and distinctive different sizes between SCNF and PEDOT—are expected to favor the formation of more ordered ladder-like polyelectrolyte complexes and, in this case, the PEDOT cations complexing optimally with the anionic sulfate groups along the lengths on the SCNF surfaces.

PEDOT:PSS/SCNF dispersions

PEDOT was synthesized by polymerization of EDOT (0.2 wt%) in the presence of PSS/SCNF. The dispersion stability of these aqueous PEDOT:PSS/SCNF complexes was assessed as a function of two experimental factors. First, the mass ratio of PSS/SCNF polyanions to PEDOT polycations was varied from 2.5 : 1 to 1.5 : 1 and 1 : 1, corresponding to respective 29, 40, and 50 wt% PEDOT in the final PEDOT:PSS/SCNF dispersions. Second, the PSS/SCNF polyanion compositions were varied to contain 0, 30, and 100% SCNF, with the remainder being PSS. The synthesized PEDOT:PSS/SCNF dispersions were diluted to a total concentration of 0.2 wt%, left in glass vials for 21 days under ambient conditions, and then inverted for observation of their stability (Fig. 3).

These aqueous PEDOT:PSS/SCNF complexes were referred to by their compositions as “PEDOT_< anion-to-cation w/w ratio >_< %SCNF in polyanion >”. PEDOT_2.5_0% showed very little sedimentation. This is to be expected, given that this sample corresponds to the PEDOT:PSS composition most commonly reported, as well as the sample with the highest 5.8 anion/cation charge ratio among all studied. With lowered anion:PEDOT ratios, PEDOT_1.5_0% and PEDOT_1_0% showed significantly more sedimentation than any other compositions, despite the fact that both still contained significant excess of anions with 3.5 and 2.3 respective anion/cation charge ratios. With 30% SCNF in the polyanion, very little sedimentation was observed in PEDOT_2.5_30%, PEDOT_1.5_30%, and PEDOT_1_30%, despite significantly reduced excess of anions in these dispersions (4.6, 2.8, and 1.9 anion/cation charge ratios). Similarly, very little sedimentation was observed in PEDOT_2.5_100% and PEDOT_1.5_100%, *i.e.*, PEDOT synthesized in the presence of SCNF serving as the sole polyanions. However, PEDOT_1_100% exhibited a thick layer of grainy sediment. Notably, this is the only composition in which the anion/cation charge ratio was below unity, being 0.77; poor dispersion stability is therefore expected. The fact that the PEDOT:PSS/SCNF dispersions with 30% SCNF in the anion showed reduced settlement compared to analogous PEDOT:PSS, despite their lower excess of anions, can be attributed to the polar unfunctionalized hydroxyl groups remained on the SCNF surfaces that aid the aqueous dispersion of PEDOT:PSS/SCNF complexes.

Properties of PEDOT:PSS/SCNF complexes

Further characterization of aqueous PEDOT:PSS/SCNF dispersions focused predominantly on those synthesized with a 2.5 : 1

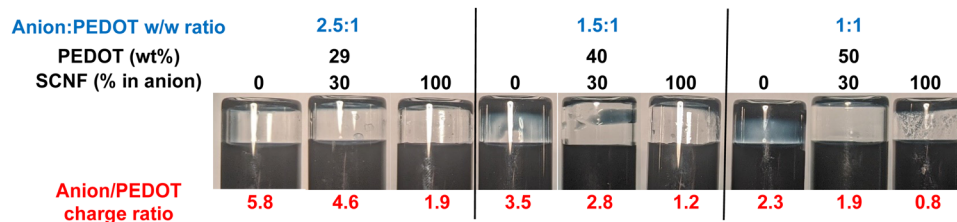


Fig. 3 Aqueous PEDOT:PSS/SCNF complexes in varied SCNF/PSS polyanion and PEDOT polycation compositions (w/w ratio) and SCNF (%) in polyanions.

polyanion/polycation w/w ratio. This subset of samples was chosen because the 2.5:1 PEDOT/polyanion w/w ratio is the most prevalent throughout the literature, allowing for the best comparison among works. The rheology of PEDOT:PSS/SCNF dispersions was, unsurprisingly, found to display more characteristics typical of SCNF as its loading was increased. Specifically, higher SCNF fractions led to an increase in overall viscosity coupled with stronger shear thinning behaviors (Fig. 4(a)). Part of this shear thinning behavior can be attributed to the strong tendency of SCNF to align themselves parallel to the direction of shearing. Certain processing techniques that rely on or induce high levels of shearing, such as film coating by doctor blading or fiber formation *via* wet spinning, could leverage this tendency to intentionally induce and control anisotropy in the fabricated materials. In the case of PEDOT:PSS/SCNF dispersions, alignment of PEDOT chains along the lengths of SCNFs has the potential to significantly increase conductivity along the nanofibril axis.

The TGA of PEDOT:PSS/SCNF complexes indicated increased thermal decomposition with higher SCNF loadings (Fig. 4(b)). Similar to other chemical processes to generate CNFs, sulfation also compromises the thermal stability of SCNF.²⁹ At and above 70% SCNF loading in the polyanion, significant loss of mass was observed at around 250 °C, below the maximum temperatures at which PEDOT is resistance stable (*ca.* 280 °C),³ reducing the viable operating temperature range of these SCNF rich dispersions. PEDOT_2.5_10%, with a much smaller loading, showed a

TGA curve more comparable to pure PEDOT:PSS with mass losses beginning closer to 280–300 °C.

Morphologies of PEDOT:PSS/SCNF complexes

The PEDOT:PSS/SCNF complexes observed under AFM and TEM showed stark differences in their arrangement depending on whether PSS was present in the dispersions. With SCNF as the sole polyanion in the system, PEDOT_2.5_100% exhibited a string-of-beads like morphology (Fig. 5(a) and (d)). The large aggregates are presumed to be PEDOT-rich regions seemingly attached to SCNF surfaces and interspersed among individual SCNFs. However, PEDOT_2.5_90%, with only 10% PSS in the anion, exhibited a completely different morphology, with only individual fibrils but no aggregate (Fig. 5(b) and (e)). In this case, it stands to reason that PEDOT is well dispersed among SCNF/PSS polyanions and likely located on the SCNF surfaces. PEDOT_2.5_30%, containing even more PSS, exhibited showed the same result, with no large PEDOT aggregates observed (Fig. 5(c) and (f)). TEM contrast for this sample was significantly poorer though, possibly due to the presence of significant amounts of PSS interfering with the uranyl acetate staining of SCNF. However, AFM appears to show thicker nanofibrils covered in small spherical beads, presumably PEDOT and PSS associated with and arranged along the SCNF surfaces (Fig. 5(c)). These structures bear a close resemblance to AFM observation of PEDOT:PSS mixed with carboxymethylated CNF in a prior work.²¹

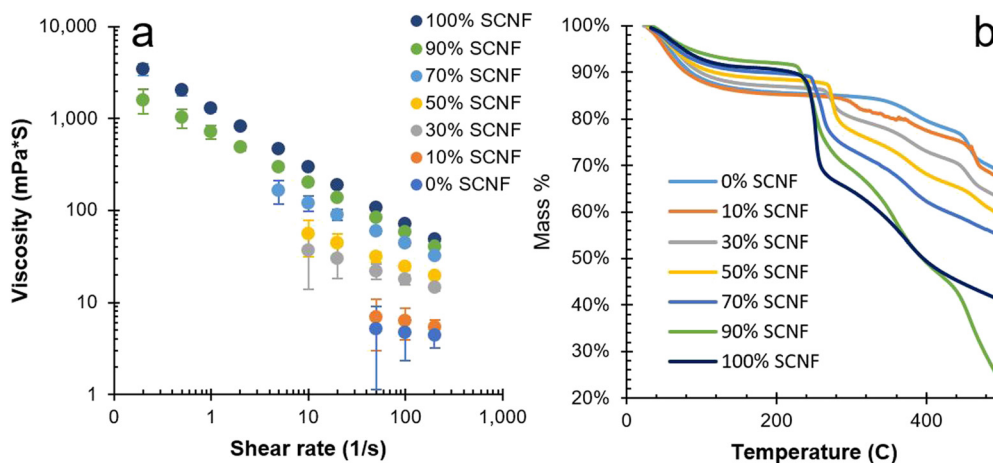


Fig. 4 Characteristics of PEDOT:PSS/SCNF complexes with 2.5:1 polyanion:PEDOT ratio: (a) viscosity vs. shear rate of 0.8 wt% dispersions; (b) TGA curves.

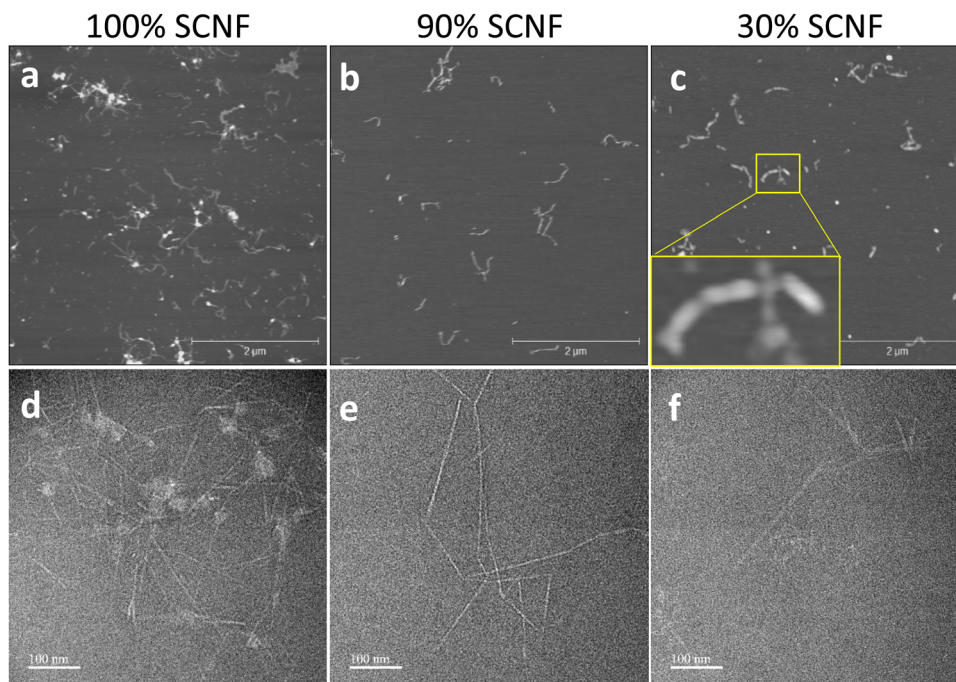


Fig. 5 PEDOT_2.5_100%, PEDOT_2.5_90%, and PEDOT_2.5_30% (a)–(c) AFM; (d)–(f) TEM. Inset in (c) shows PEDOT/PSS associated along SCNFs.

Conductivity of films cast from PEDOT:PSS/SCNF complexes

Films cast from aqueous PEDOT_2.5_0% (*i.e.* 2.5 PEDOT:PSS) exhibited a conductivity of 0.048 S cm^{-1} (Fig. 6(a), and Fig. S2, ESI[†]). PEDOT_2.5_10% showed identical conductivity despite the inclusion of 10% SCNF. Intriguingly, as the SCNF loading was increased to 30%, PEDOT_2.5_30% showed a conductivity of 0.14 S cm^{-1} , a nearly 3-fold increase. This improvement could be attributed to the optimal organization induced in PEDOT and PSS through their associations on the SCNF surface and along the length of the fibrils, creating an ordered, longer, and more cohesive conductive pathway. Higher SCNF loadings of 50%, 70%, 90%, or 100% showed no additional improvement in conductivity, with values which were higher than that

of PEDOT_2.5_0% but either lower than or similar to that of PEDOT_2.5_30% within the margin of error.

The addition of either EG or DMSO as secondary dopants revealed a different trend. Most significantly, the effect of secondary dopants on the conductivity of PEDOT:PSS/SCNF systems was found to depend predominantly on the amount of PSS in the polyanions (Fig. 6(b)). Adding either 5 wt% EG or DMSO to PEDOT_2.5_0% significantly increased the conductivity of their cast films, from 0.048 S cm^{-1} to 23.8 S cm^{-1} or 10.0 S cm^{-1} , respectively. This increase of more than two orders of magnitude falls in line with the enhancement factors previously reported for commercial PEDOT:PSS or Clevis PH 1000.¹⁴ The EG treated film PEDOT_2.5_10% had a maximum conductivity of 37.5 S cm^{-1} , the

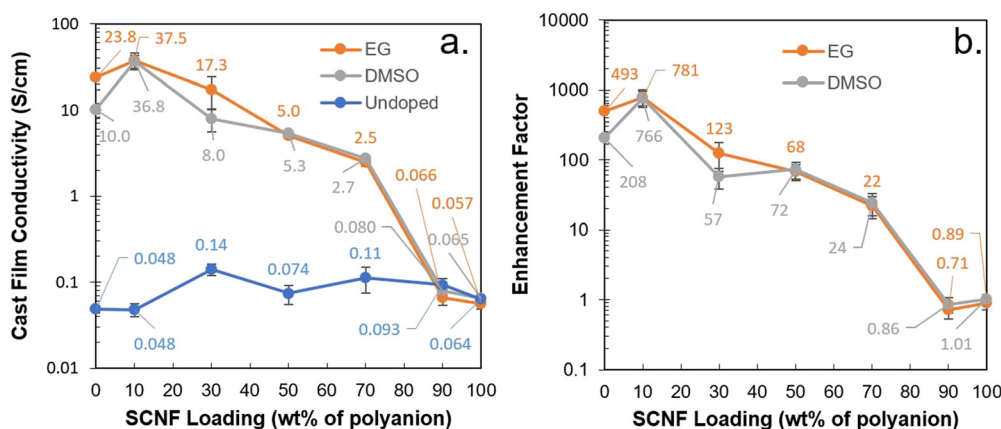


Fig. 6 Conductivity of films cast from PEDOT:PSS/SCNF complexes at 2.5:1 w/w polyanion/PEDOT ratio and varying PSS/SCNF polyanions as the host polyelectrolytes: (a) conductivity of cast films as is and secondary doping with EG and DMSO; (b) enhancement factor from secondary dopants of films in a.

highest among all compositions in this work and 58% higher in conductivity than EG treated PEDOT_2.5_0%. However, as SCNF loading in the polyanions was increased to 30% and above, the conductivity of EG and DMSO treated films progressively decreased. EG treatment of films cast from PEDOT_2.5_90% and PEDOT_2.5_100% gave an enhancement factor of near unity, indicating no significant change in conductivity. These observations allude to the fact that secondary doping acts on the PSS in the system, rather than having a direct effect on the PEDOT. Of the previously suggested explanations, this observation also supports the notion that secondary dopants act somewhat as plasticizers, allowing PSS chains to flow and phase separate from PEDOT during curing.¹⁷ As a consequence, maximizing the conductivity of hybrid PEDOT:PSS/SCNF complexes entails balancing the co-polyanion ratios in order to leverage the alignment effect of SCNF without compromising the effects of secondary doping on PSS. This same principle is postulated to be potentially applicable to other polyanionic cellulose nanofibrils in mixing with commercial PEDOT:PSS dispersions, though the use of secondary dopants and their effect in relation to undoped dispersions has not been studied. In the present work, approximately 10% SCNF in the anion was found to be the optimal loading wherein the combined effects of secondary doping and SCNF inclusion lead to films with higher conductivity than PEDOT:PSS alone.

To get an idea for how the PEDOT content affects electrical performance, the conductivity of PEDOT:PSS/SCNF films from dispersions at varying polyanion/PEDOT mass ratios, both with and without EG treatment, was also further explored (Fig. S2, ESI†). Increasing the amount of conducting PEDOT in the dispersion yielded no clearly observable increase in conductivity. Regardless of the amount of PEDOT, EG addition also yielded no substantial changes in conductivity for the samples with no PSS, again affirming the central role of PSS in secondary doping. What these results further emphasize is that films based off of PEDOT:PSS/SCNF polyelectrolyte complexes were heterogeneous, and their conductivity depends heavily on the supramolecular ordering beyond varying the fraction of conducting material or doping level alone. As demonstrated by this systematic investigation of PEDOT polyelectrolyte complexes, further improvement in conductivity may be limited by their isotropic structure and lacking the tools and understanding to effectively optimize the interconnected relationships between these parameters.

Wet-spun PEDOT:PSS/SCNF fibers

A unique characteristic of 1D nanomaterials like SCNF is their anisotropy and ability to be oriented through the use of shear force to potentially create additional anisotropy in materials. To exploit the SCNF's ability to facilitate orientation of PEDOT, fibers were wet spun at 0.03 mL min⁻¹ from an aqueous dispersion of PEDOT_2.5_30% (Fig. 7). While 10% SCNF loading was found optimal for film formation, the higher 30% SCNF loading was chosen for fiber spinning to provide greater anisotropy and differentiation from PEDOT:PSS. Fibers spun into acetone had 10–14 μm diameters and boasted a

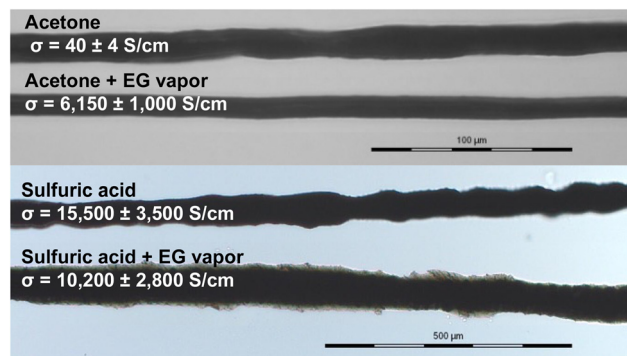


Fig. 7 Optical microscopy and conductivities of fibers wet-spun from PEDOT:PSS/SCNF (30 wt% SCNF in the polyanion and 2.5 : 1 polyanion/PEDOT ratio) into acetone or 72 wt% sulfuric acid, with and without EG vapor treatment.

conductivity of $40 \pm 4 \text{ S cm}^{-1}$ without secondary doping, 285 times the conductivity of the 2D cast films (0.14 S cm^{-1}). It should be noted that the significant thixotropy²⁵ of SCNF, a quality which they imparted to the PEDOT:PSS/SCNF dispersions, presented challenges for continuous wet-spinning process at the laboratory scale. The intense shearing that occurred during filtration and degassing of the spin dope rendered it homogeneous and spinnable, yet as spinning progressed the viscosity visibly increased as the dope began to gel. Upscaling fiber spinning would require controlling the viscosity and thixotropy of the aqueous PEDOT:PSS/SCNF spin dopes.

Upon exposure to EG vapor for 24 hours, the fiber conductivity was significantly increased to $6150 \pm 1000 \text{ S cm}^{-1}$, a more than 150-fold improvement over the undoped fibers. The EG treated fiber is over 355 times more conductive compared to EG treated films cast from the same dispersion (17.3 S cm^{-1}). A second fiber was spun by hand from the same spin dope into a Petri dish containing 72 wt% sulfuric acid. This fiber boasted an even higher conductivity of $15500 \pm 3500 \text{ S cm}^{-1}$. Curiously, EG vapor treatment on the sulfuric acid coagulated fiber reduced the conductivity to $10200 \pm 2800 \text{ S cm}^{-1}$, indicating that sulfuric acid is likely a more efficacious secondary dopant than EG, with the added benefit of serving simultaneously as a coagulant. The fibers were more irregular than those spun into acetone *via* syringe pump into a larger acetone bath, however. Therefore, while hand spinning aqueous PEDOT:PSS/SCNF into sulfuric acid demonstrated the promise of this strategy, special equipment designed to control spinning and handle sulfuric acid safely would be necessary for further scaleup of this process.

The impressive 6150 S cm^{-1} conductivity of the fiber coagulated in acetone and treated with EG is nearly double the 3131 S cm^{-1} conductivity reported previously for fibers spun from commercial PEDOT:PSS (Clevios PH1000) into a 50/50 v/v% isopropanol and acetone mixture, drawn, and treated with EG.³⁰ Similarly, the fiber coagulated in sulfuric acid and boasting an even more impressive conductivity of 15500 S cm^{-1} is over 4× the conductivity of fibers spun from commercial PEDOT:PSS into concentrated sulfuric acid.³¹ The 15500 S cm^{-1} conductivity of fiber coagulated in sulfuric acid is the most conductive PEDOT fiber reported to date, to our knowledge. These results showcase the efficacy of

shear-mediated alignment of PEDOT by the highly anisotropic and shear-thinning SCNF and the effectiveness of 72 wt% sulfuric acid serving as dual coagulant and secondary dopant for boosting electrical performance. Wet spinning directly into concentrated sulfuric acid has the potential to fabricate fibers with even higher conductivity and to be scaled up similar to the commercial production of poly(1,4-phenylene terephthalamide), though with the solvent and coagulant inverted. Additional improvements to fiber mechanical and electrical performance might be achieved with the addition of a drawing step, which has been reported on PEDOT:PSS fibers previously.³²

Conclusions

This study has demonstrated how supramolecular structuring and ordering of heterogeneous PEDOT:PSS complexes could be aided by SCNF and optimized to significantly improve their electrical conductivities in the forms of 1D and 2D conductors. Alignment of PEDOT along the surfaces of 1D nanomaterials was induced by the highly anisotropic SCNFs with 1.8 mmol g⁻¹ surface charge, whose anionic charge spacing closely matches that of the PEDOT cations. Simple inclusion of 30 wt% SCNF in the PSS/SCNF polyanions improved the conductivity of 2D films from PEDOT:PSS/SCNF complexes threefold, from 0.048 to 0.14 S cm⁻¹. With added ethylene glycol, films from PEDOT:PSS/SCNF synthesized with a 10% SCNF polyanion exhibited the highest conductivities of 37.5 S cm⁻¹; 58% higher than the film from the control without SCNF (23.8 S cm⁻¹) and, most significantly, nearly 800 times the 0.048 S cm⁻¹ conductivity of the undoped films with SCNF. Systematic evaluation of EG and DMSO as secondary dopants gave clear evidence to support the theory that they act on PSS to improve the conductivity of films cast from aqueous PEDOT:PSS/SCNF complexes. The inclusion of small quantities of SCNF as a co-polyanion further facilitated the effect of the secondary dopants. Templating PEDOT with 30 wt% high aspect ratio SCNF led to its greater degree of orientation along the fiber axis to reach exceptionally high conductivity of 6150 ± 1000 S cm⁻¹ when spun into acetone and treated with EG vapor and 15 500 ± 3500 S cm⁻¹ when spun into 72% sulfuric acid that served as dual coagulating and doping agent. These observations on 1D fibers wet spun from aqueous PEDOT:PSS/SCNF complexes highlight the importance of molecular orientation aided by SCNF and the immense benefit of streamlining the coagulation and doping processes into one by using sulfuric acid as dual coagulant and dopant while achieving unprecedented levels of conductivity. The significant thixotropy of SCNF, as proven in lab scale operation, present broad range of processing prospects for aqueous PEDOT:PSS/SCNF dispersions, such as ink-jet printing, silk screen, additive engineering, or blade coating.

Experimental

Materials

Anhydrous *N,N*-dimethylformamide (DMF), sodium persulfate, iron(III) sulfate monohydrate, and poly(styrene sulfonic acid)

(75 kDa, aqueous, 18 wt%) were purchased from Sigma-Aldrich. 3,4-Ethylenedioxythiophene (99%) was purchased from Acros. Sodium hydroxide (1.00 N solution) was purchased from Spectrum Chemical. Chlorosulfonic acid (99%) was purchased from Alfa Aesar. Ethylene glycol (EG), dimethyl sulfoxide (DMSO), acetone, and sodium hydroxide (NaOH, 1.00N solution) were purchased from Fischer Scientific. Sheets of softwood dissolving pulp cellulose were received from the US Forest Product Laboratory of the US Forest Service in Madison, WI. Ultra-pure water was acquired from a Milli-Q Advantage A10 water purification system. Regenerated cellulose dialysis tubing (3 kDa molecular weight cutoff) was purchased from Spectrum Laboratories. Silver conductive epoxy was purchased from MG Chemicals. Unless otherwise specified, all chemicals were utilized as-is.

Synthesis and characterization of sulfated cellulose nanofibrils

SCNF was produced from dissolving pulp cellulose through a previously reported procedure. Cellulose pulp sheets (1.0 g) were torn into squares with sides of 1 cm or smaller and placed in a 50 mL round-bottom flask. Anhydrous DMF (45 mL) was added to the flask and the cellulose pulp was allowed to disperse under vigorous stirring for 2 hours. Chlorosulfonic acid (1.25 moles per mole of anhydroglucose, AGU) was added dropwise to 5 mL of anhydrous DMF chilled in an ice bath to prevent excessive heating. This acid/DMF mixture was added to the dispersed pulp and the reaction was allowed to proceed for 45 minutes. Termination was carried out through the addition of 10 mL of purified water, after which the cellulose sulfate product was washed with more water by repeated centrifugation and decanting. Residual DMF and acid was removed through dialysis against purified water changed daily for a period of approximately one week, until the conductivity of the dialyzing water plateaued below 1 μS cm⁻¹. Sulfated cellulose was disintegrated by 10 minutes of high-speed blending (Vitamix 5200, 30 000 rpm) at a concentration of 0.2 wt%. Blending was performed in 5 minute increments with cool-down periods between to avoid excessive heating. SCNF was concentrated as needed using a rotary evaporator.

The height and length of SCNF were assessed using atomic force microscopy (AFM) (Asylum Research MFP-3D) using OMCL-AC160TS standard silicon probes with a nominal tip radius of 7 nm and spring constant of 26 N m⁻¹. Several drops of SCNF diluted to 0.00003 wt% were deposited on freshly cleaved mica disks and dried under ambient conditions. AFM surface profiles were collected in AC mode and processed using the open-source programs Gwyddion and ImageJ to determine fibril dimensions. The width of SCNF was additionally assessed using transmission electron microscopy (TEM). Aqueous SCNF was diluted to 0.01 wt% and deposited on a glow discharged TEM grid (carbon/formvar over 300 mesh copper). After 10 minutes the excess was blotted off and the samples were repeatedly stained with 2 wt% uranyl acetate. Micrographs were taken at 50 000× magnification on a JEOL JEM 2100F-AC TEM. Micrographs were analyzed with the program imageJ, with SCNF widths being determined by finding the full width at half maximum (FWHM) of the intensity profiles across fibrils.

SCNF charge was determined through conductometric titration. SCNF was dialyzed again against purified water for several days to remove small-molecule contaminants, after which it was run through an ion exchange column loaded with a strong acid exchange resin (DOWEX Marathon C) to ensure that the sulfate half-ester groups were in their acid form. Titration was carried out with 0.01 M NaOH and the equivalence point was determined by finding the minima in the conductivity curve where all acidic sulfate groups were neutralized.

The crystallinity of the dissolving pulp cellulose and all nanocellulose samples was determined through X-ray diffraction (XRD, Fig. S3, ESI†). Films of SCNF approximately 10 μm thick were made by depositing 10 mL of SCNF at a concentration of 0.2 wt% in a glass dish and allowing it to dry at 50 °C. The dissolving pulp was ground and deposited as a powder on an XRD sample stage using a very small amount of high-vacuum grease. Scans were collected of the films/powder on a Bruker D8 Advance Eco diffractometer with a Cu K α radiation source. Samples were scanned at 2θ values ranging from 5° to 40° with an angular increment of 0.03° and a scan time of 2.5 s per increment. Crystallinity index (CrI) was estimated from XRD *via* a peak deconvolution with four crystalline peaks and the fitting software Fityk,³³ with each peak being modeled using a Voigt function.

Syntheses of PEDOT:PSS:SCNF Complexes

All PEDOT complexes were synthesized through the chemical polymerization of EDOT in the presence of either SCNF, PSS, or some mixture thereof. The amount of EDOT in each reaction was kept constant to maintain an aqueous concentration of 0.2 wt%, near its aqueous solubility limit. The amount of either SCNF or PSS polyanion or total SCNF/PSS polyanions were varied to achieve 2.5:1, 1.5:1, or 1:1 polyanion:PEDOT w/w ratios. The composition of the polyanion was also varied, consisting of 0, 10, 30, 50, 70, 90, or 100 wt% SCNF, with any remainder being PSS.

For a typical reaction, the polyanion or polyanions (0.1–0.25 g) were added to a 50 mL round bottom flask and purified water was added to reach a total volume of 50 mL. EDOT (0.1 g) was added and allowed to dissolve for two hours under magnetic stirring. The mixture was degassed *via* 10 minutes of sonication (Branson 2510 bath sonicator) and the reaction was initiated by adding sodium persulfate (0.234 g) as an oxidizing agent and a small amount of ferric sulfate catalyst (10.5 mg). Reactions were allowed to proceed for a period of 24 hours, at which point the PEDOT complexes were adjusted to neutral pH with 1 M NaOH and purified *via* dialysis against ultra-pure water using regenerated cellulose dialysis tubing. Once the conductivity of the dialyzing water plateaued, the complexes were concentrated using a rotary evaporator to 0.8 wt%.

Characterization of PEDOT complexes

PEDOT:SCNF and PEDOT:PSS:SCNF were imaged by AFM with a procedure similar to the one detailed for SCNF. PEDOT complexes were diluted to 0.00008 wt%, deposited on mica, and scanned using an Asylum Research MFP-3D atomic force

microscope. TEM micrographs were collected and analyzed for PEDOT:PSS and PEDOT:PSS:SCNF dispersions utilizing a procedure analogous to that outlined previously for the analysis of SCNF.

The viscosity of aqueous PEDOT dispersions was measured using a Brookfield DV3T rheometer with a concentric circle geometry. PEDOT dispersions were concentrated to 0.8 wt% *via* rotary evaporation. Viscosity measurements were taken at 25 °C at 0.1 to 200 s⁻¹ shear rates.

Films of PEDOT complexes were cast on 2.5 cm by 2.5 cm glass first cleaned through sonication in acetone, then rinsed in isopropanol (Fig. S3, ESI†). The glass substrates were soaked in 30% nitric acid for a period of at least 24 hours to increase surface hydrophilicity prior to casting. Films of PEDOT dispersions were deposited through drop casting 250 μL of aqueous dispersion at a concentration of 0.8 wt%, either as-is or with the addition of 5 w/v% EG or DMSO to act as secondary dopants. Films were allowed to dry in air and then cured at 120 °C for 60 minutes. For most conditions, films were made in duplicate.

The resistivity of films was measured using the four-point probe method with colinear probes. For each film, at least 3 resistivity measurements were taken for each film and averaged. Film thickness was measured by using AFM as a stylus profilometer, measuring the height difference between the bulk of the film and the substrate surface in several locations along a scored groove. Two height measurements were taken for each film in different locations and averaged. Conductivity was calculated from thickness and resistivity measurements according to the equation $\sigma = 1/(R \cdot t)$, where σ is conductivity, R is the sheet resistance of the film, and t is the film thickness.²²

The thermal decomposition of PEDOT:PSS/SCNF complexes was assessed using thermogravimetric analysis (TGA). Dispersions at 0.8 wt% were oven dried overnight at 50 °C. Between 3 and 5 mg of these dispersions were placed in a platinum pan and analyzed using a Shimadzu TGA-50 in a nitrogen environment with a heating rate of 10 °C min⁻¹ and a maximum temperature of 500 °C.

Wet spinning of PEDOT:PSS/SCNF dispersions

PEDOT_2.5_30% was concentrated to 1.38 wt% *via* rotary evaporation. The dispersion was run through a syringe filter with 5 μm pores to remove small particulates and degassed using a bath sonicator for 5 minutes. Wet spinning was carried out by extruding the dispersion through a g27 needle (ID = 210 μm) directly into a 1L beaker filled with acetone at a rate of 0.03 mL min⁻¹ controlled by a syringe pump. The coagulated fiber was wound onto a 3 cm diameter cylindrical collector without tension using a DC electric motor. Fibers were oven dried overnight at 50 °C. A portion of the dried fibers were exposed to EG vapor by placing them in a glass jar with an open dish of EG at 50 °C for 24 hours. Both the EG treated and untreated fibers were cured at 120 °C for 60 minutes.

An additional fiber was spun by hand from the same dispersion using the same size needle into a Petri dish containing 72 wt% sulfuric acid. This fiber was allowed to coagulate for approximately 30 seconds, rinsed in a water bath, and air dried.

A portion of the dry fiber was subjected to EG vapor treatment and curing identically to the acetone-coagulated fiber described above.

The diameter of the fibers was measured using optical microscopy. The conductivity of the fibers was measured using the two-point probe method by first mounting the fibers using conductive epoxy with a distance of 1 cm between epoxy electrodes and measuring the resistance between points using a multimeter. Resistance (R) measurements were converted to conductivity (σ) with the equation $\sigma = L/(RA)$, where A is the cross-sectional area of the fiber. Three measurements were taken in different locations along each fiber and averaged.

Author contributions

BP and YLH conceptualized the framework. BP conducted experiments and wrote the first draft of manuscript. YLH revised. BP and YLH edited.

Conflicts of interest

The authors declare no competing financial interest.

Acknowledgements

The United States Department of Defense's Science, Mathematics, and Research for Transformation (SMART) scholarship and financial support from the USDA National Institute of Food and Agriculture (CA-D-6706) are greatly appreciated.

References

- 1 BAYER AG OP – DE 3813589 A OP – DE 3843412 A, EP 0339340 A2, 1989.
- 2 T. Nezakati, A. Seifalian, A. Tan and A. M. Seifalian, *Chem. Rev.*, 2018, **118**, 6766–6843.
- 3 A. Elschner, S. Kirchmeyer, W. Lovenich, U. Merker and K. Reuter, *PEDOT: principles and applications of an intrinsically conductive polymer*, CRC Press, 2010.
- 4 Y. Kudoh, K. Akami and Y. Matsuya, *Synth. Met.*, 1999, **102**, 973–974.
- 5 A. M. Nardes, M. Kemerink, R. A. J. Janssen, J. A. M. Bastiaansen, N. M. M. Kiggen, B. M. W. Langeveld, A. J. J. M. Van Breemen and M. M. De Kok, *Adv. Mater.*, 2007, **19**, 1196–1200.
- 6 F. Pädinger, C. J. Brabec, T. Fromherz, J. C. Hummelen and N. S. Sariciftci, *Opto-Electronics Rev.*, 2000, **8**, 280–283.
- 7 L. Huang, Z. Hu, K. Zhang, P. Chen and Y. Zhu, *Thin Solid Films*, 2015, **578**, 161–166.
- 8 M. Eslamian and F. Soltani-Kordshuli, *J. Coatings Technol. Res.*, 2018, **15**, 271–280.
- 9 Z. Xiong and C. Liu, *Org. Electron.*, 2012, **13**, 1532–1540.
- 10 J. Zhou, E. Q. Li, R. Li, X. Xu, I. A. Ventura, A. Moussawi, D. H. Anjum, M. N. Hedhili, D. M. Smilgies, G. Lubineau and S. T. Thoroddsen, *J. Mater. Chem. C*, 2015, **3**, 2528–2538.
- 11 A. G. MacDiarmid and A. J. Epstein, *Synth. Met.*, 1994, **65**, 103–116.
- 12 M. Döbbelin, R. Marcilla, M. Salsamendi, C. Pozo-Gonzalo, P. M. Carrasco, J. A. Pomposo and D. Mecerreyes, *Chem. Mater.*, 2007, **19**, 2147–2149.
- 13 B. Fan, X. Mei and J. Ouyang, *Macromolecules*, 2008, **41**, 5971–5973.
- 14 J. Ouyang, Q. Xu, C. W. Chu, Y. Yang, G. Li and J. Shinar, *Polymer*, 2004, **45**, 8443–8450.
- 15 J. L. Brédas and G. B. Streets, *Acc. Chem. Res.*, 1985, **18**, 309–315.
- 16 J. Y. Kim, J. H. Jung, D. E. Lee and J. Joo, *Synth. Met.*, 2002, **126**, 311–316.
- 17 L. A. Pettersson, S. Ghosh and O. Inganäs, *Org. Electron.*, 2002, **3**, 143–148.
- 18 S. K. M. Jönsson, J. Birgeron, X. Crispin, G. Greczynski, W. Osikowicz, A. W. Denier van der Gon, W. R. Salaneck and M. Fahlman, *Synth. Met.*, 2003, **139**, 1–10.
- 19 J. Ouyang, C. W. Chu, F. C. Chen, Q. Xu and Y. Yang, *Adv. Funct. Mater.*, 2005, **15**, 203–208.
- 20 B. Thomas, M. C. Raj, B. K. Athira, H. M. Rubiyah, J. Joy, A. Moores, G. L. Drisko and C. Sanchez, *Chem. Rev.*, 2018, **118**, 11575–11625.
- 21 D. Belaineh, J. W. Andreasen, J. Palisaitis, A. Malti, K. Håkansson, L. Wågberg, X. Crispin, I. Engquist and M. Berggren, *ACS Appl. Polym. Mater.*, 2019, **1**, 2342–2351.
- 22 J. Zhou and Y.-L. Hsieh, *ACS Appl. Mater. Interfaces*, 2018, **10**, 27902–27910.
- 23 S. Zhou, Z. Qiu, M. Strømme and Z. Wang, *Adv. Funct. Mater.*, 2020, **30**, 1–9.
- 24 X. Feng, X. Wang, M. Wang, S. Zhou, C. Dang, C. Zhang, Y. Chen and H. Qi, *Chem. Eng. J.*, 2021, **418**, 129533.
- 25 B. Pingrey and Y.-L. Hsieh, *Biomacromolecules*, 2022, **23**, 1269–1277.
- 26 K. Zhang, E. Brendler, A. Geissler and S. Fischer, *Polymer*, 2011, **52**, 26–32.
- 27 E. G. Kim and J. L. Brédas, *J. Am. Chem. Soc.*, 2008, **130**, 16880–16889.
- 28 A. Rembaum, *J. Macromol. Sci., Part A: Pure Appl. Chem.*, 1969, **3**, 87–99.
- 29 S. Camarero Espinosa, T. Kuhnt, E. J. Foster and C. Weder, *Biomacromolecules*, 2013, **14**, 1223–1230.
- 30 J. Zhou, M. Mülle, Y. Zhang, X. Xu, E. Q. Li, F. Han, S. T. Thoroddsen and G. Lubineau, *J. Mater. Chem. C*, 2016, **4**, 1238–1249.
- 31 J. Zhang, S. Seyedin, S. Qin, P. A. Lynch, Z. Wang, W. Yang, X. Wang and J. M. Razal, *J. Mater. Chem. A*, 2019, **7**, 6401–6410.
- 32 R. Sarabia-Riquelme, M. Shahi, J. W. Brill and M. C. Weisenberger, *ACS Appl. Polym. Mater.*, 2019, **1**, 2157–2167.
- 33 S. Park, J. O. Baker, M. E. Himmel, P. A. Parilla and D. K. Johnson, *Biotechnol. Biofuels*, 2010, **3**, 10.